Robotica (2010) volume 28, pp. 1045–1056. © Cambridge University Press 2010
doi:10.1017/S0263574709990907

A smart hydraulic joint for future implementation in robotic structures

J. Berring†, K. Kianfar†, C. Lira‡, C. Menon†* and F. Scarpa‡

†*MENRVA Group, School of Engineering Science, Simon Fraser University, 8888 University Dr., Burnaby, BC, V5A 1S6, Canada*
‡*Department of Aerospace Engineering, University of Bristol, UK*

(Received in Final Form: December 14, 2009. First published online: January 18, 2010)

SUMMARY
A hydraulic flexible joint inspired by the actuation system of spiders is investigated in this paper. Its design and characteristics are discussed and a mathematical model is developed to describe its static behaviour. Results of experimental tests are presented to validate its performance. A comparison to other hydraulic actuation systems is performed. The use of the proposed hydraulic flexible joint in adaptive robotic structures is addressed and discussed.

KEYWORDS: Hydraulic system; Smart actuator; Flexible structure.

NOMENCLATURE

L	Distance between subsequent spacers (length of the bay in which the tube is inserted)
w	Width of the flexible beam
h_1	Height of the tube in contact with the spacer (see Fig. 7(a))
R	Resultant of the tube action due to the pressurization of the working fluid
$p = RA$	Reference pressure
$A = h_1 w$	Active area
T	Resultant of the tube action on spacers when the working fluid is not pressurized
$p^* = RA + TA$	Pressure causing joint torque
C	Centre of rotation of the joint (see Fig. 2)
h	Distance of R from the centre of rotation C
F	Applied external force
s	Distance of F from the centre of rotation C
$\tau_{\mathrm{LOAD}} = F\,s$	Applied external torque
First instance	Case in which the robot lifts a leg
Second instance	Case in which all the legs are in contact with the ground and support the whole weight of the robot
x	Distance from the left-hand side of the flexible joint (see Fig. 7(a))
$y(x)$	Vertical deflection
$M(x)$	Bending moment acting on the beam
E	Young's modulus of the material
I	Second moment of area
t	Thickness of the beam
τ	Torque exerted by the expansion of one tube
${}^i\theta$	Rotation due to the deflection of i modules
W_l	Robot weight acting upon one leg
θ_M	Maximum angular rotation of the joint
y_M	Maximum deflection of the joint end
p_L	Pressure needed to lift the leg
$H[\xi]$	Heaviside step function

* Corresponding author. E-mail: cmenon@sfu.ca

1. Introduction

The development of modern technologies in different fields such as industrial manufacturing, transport, services, housing facilities, public security and space exploration, stimulates the exploitation of new bioinspired concepts and ideas. By taking inspiration from the hydraulic systems of spiders,[1] a flexible hydraulic joint suitable for being embedded on adaptive robotic structures has recently been proposed and investigated by the authors.[2–5,40] On the other hand, miniaturized hydraulic systems have been developed by several researchers for actuating anthropomorphic hand prostheses,[6–11] robotic catheters,[7–17] self-propelling endoscopes,[18,19] macro-scale hexapod robots,[20–23] surgical robotic systems,[24–26] and several other devices. Different kinds of micro-actuation systems have been investigated[27,28] and several micro-pump systems have been manufactured and their performances compared.[29,30]

In this paper, a prototype of the flexible hydraulic flexible joint[40] is investigated and a model is derived. The paper is organized as follows: Section 2 presents the bio-inspired design; Section 3 presents the simplified model of the engineered hydraulic joint. In Section 4, a macro-scale prototype is described and its performance discussed; in Section 5, a mathematical model of the joint is derived. The last section draws conclusions and presents future directions.

2. Proposed Bio-Inspired Design

Legs of several arthropods (arachnids, diplopods, chilopods, and pauropods) have joints which, from an engineering perspective, can be classified as hinge joints. The anatomic

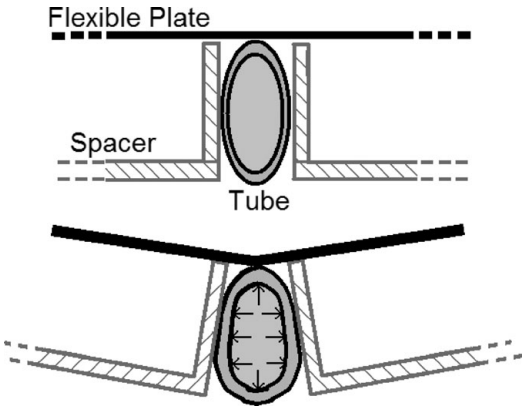

Fig. 1. Cross section of a single module of the hydraulic joint.

form of their joints often does not permit the presence of extensors. The empty spaces in-between muscles and skeleton are filled in with haemolymph (spider's blood), which can be pressurized to achieve leg extension. The methodology used by various spiders and whipscorpions to extend their legs is well documented.[1,2] It is worth mentioning that each leg of a spider can have up to 10 degrees-of-freedom (DOF)[31] – the actuation system of spiders should therefore have excellent performance to enable fine control of such a large number of DOFs. Spider's legs are connected to the prosoma, which is the spider's central body. The extension of the legs is achieved by the contraction of the prosoma, which pressurizes the haemolymph. When the prosoma relaxes, the haemolymph flows back into the prosoma and legs recover their initial position.

The bio-inspired hydraulic joint that was conceived is shown in Fig. 1. The investigated system has a closed loop design – it uses only one continuous deformable tube to avoid any gasket and/or other sealing means; this hydraulic joint is therefore suitable to be used in a large variety of robotic applications, including those to be performed in controlled environments, such as clean rooms.[5] Figure 1(a) shows a cross-section of one module; a flexible tube is positioned in between two rigid spacers; the spacers are fixed to a flexible beam which behaves as a torsion spring. When the pressure inside the tube is increased, the tube expands and exerts a distributed force against the spacers; as a result, the flexible beam bends. Several modules can be combined together to obtain a modular joint capable of displaying large displacements. One single tube can be used for the entire multi-modular flexible joint in order to prevent any leakage of the working fluid.

3. Cantilever Model for a Single Joint

A simplified representation of a single module of the hydraulic joint is shown in Fig. 2(a). In this figure, one spacer is fixed to the ground. Figure 2(b) shows forces acting onto the joint. It is assumed that the joint rotates around a fixed point C. An external force F is applied at a distance s from the centre of rotation. The pressure p exerted by the inflated tube on the surface area A of the spacer is represented by its resultant R applied at a distance h from the centre of rotation C. In Fig. 2(b), T represents the force that the tube exerts against the spacer when there is no pressure inside the tube. It is worth remarking that the tube has a circular cross section in its relaxed configuration – when it is inserted between two spacers it assumes an elliptical cross section and provides a reaction force T.

The equilibrium of the torque around C yields

$$R = F\frac{s\,\cos\theta}{h} + \frac{k}{h}\theta - T, \tag{1}$$

where k is the rotational spring constant of a single joint. By substituting the pressure $p = R/A$, the external torque $\tau_{\mathrm{LOAD}} = F\,s$, and by considering small angles, Eq. (1) yields

$$p(\tau_{\mathrm{LOAD}}, \theta) = \left(\frac{1}{A\quad h}\right)\tau_{\mathrm{LOAD}} + \left(\frac{k}{A\quad h}\right)\theta + \left(-\frac{T}{A}\right) \tag{2}$$

or equivalently

$$p(\tau_{\mathrm{LOAD}}, \theta) = a \cdot \tau_{\mathrm{LOAD}} + b \cdot \theta + c \tag{3}$$

where a, b and c are constant values.

Equation (3) shows the relation between the pressure p, the external torque τ_{LOAD} applied to the joint and the rotation θ of the joint itself. The considered simplifications allowed obtaining a simple linear model for one module of the hydraulic flexible joint.

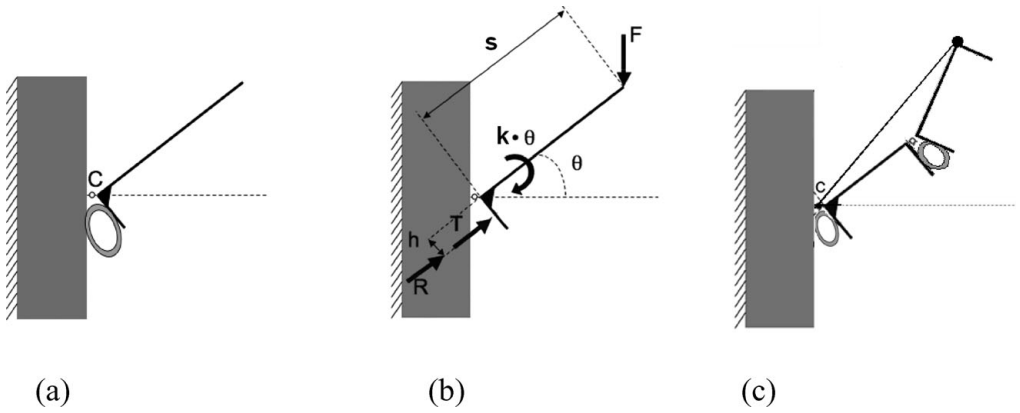

Fig. 2. Simplified representation of one module (a, b) and multiple modules (c).

https://doi.org/10.1017/S0263574709990907 Published online by Cambridge University Press

Table I. Properties of the hydraulic flexible joint.

Outer diameter (D)	Wall thickness (t_D)	Young's modulus of the tube (E_D)	Length of the bay (L)	Joint's width (w)	Thickness of the flexible beam (t)	Young's modulus of the flexible beam (E)
2.08 mm	0.25 mm	19.3 MPa	0.6 mm	50 mm	0.1 mm	193 MPa

4. Prototype

A prototype was manufactured to identify the performance of the proposed design (see Fig. 3). The tube is elastically deformed and assumes an elliptical shape when inserted into the bay (space between two subsequent rigid spacers). Measured tube size and mechanical properties are summarized in Table I.

4.1. Testing one module

One of the modules of the flexible joint shown in Fig. 3 was fixed to a vertical frame to be experimentally tested. A rigid beam was fixed to the flexible joint (see Fig. 4) and different weights were successively hung at the tip of the rigid beam to apply the external force F shown in Fig. 2. The external torque t_{load} acting on the flexible joint was computed by taking into account both the weight of the rigid beam and the weight hanging from the tip of the rigid beam. The pressure inside the tube was measured by a pressure gauge. The rotation of the joint, which was mechanically magnified by the rigid beam, was measured by taking digital images of the cantilever against a vertical measuring surface. Resolution and precision of instruments used during the experimental tests allowed obtaining measurements with a torque error of $\pm$ 7 Nmm. Table II summarizes test results. This table does not report data for pressures higher than 800 kPa due to the full-scale limit of the pressure sensor.

Figure 5 shows the experimental results from table II plotted with fitting functions. Large angles of rotation are achieved for high values of the pressure inside the tube. For increased values of the external torque, the constant rotation of the joint can be kept still by imposing higher values of pressure. A linear equation relating pressure and torque was found using a least squares fitting:

$$p(\tau_{\mathrm{LOAD}}, \theta) = 7\tau_{\mathrm{LOAD}} + b(\theta) \tag{4}$$

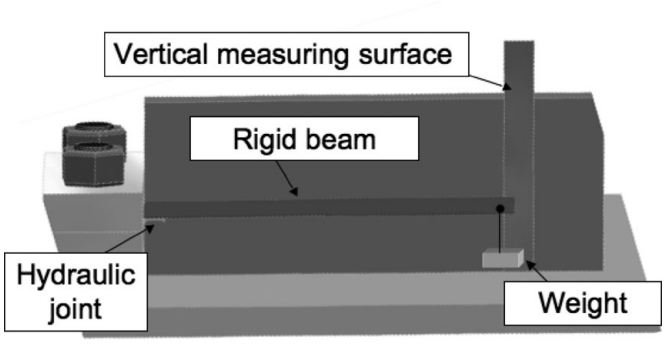

Fig. 4. Representation of the experimental setup.

Table II. Pressure (kPa) required to rotate one module of the hydraulic joint of a fixed angle (deg) when an external torque (Nmm) is applied.

External torque (Nmm)		28	36	44	51	59	67	75	91	106
Angle (deg)	6.2	**444**	**480**	**539**	**601**	**671**	**731**	**779**	–	–
	4.6	**343**	**400**	**445**	**521**	**582**	**619**	**684**	**798**	–
	3.1	**265**	**325**	**375**	**435**	**500**	**532**	**590**	**713**	–
	1.5	**190**	**205**	**290**	**351**	**401**	**446**	**501**	**605**	**712**

where p is the pressure in the tube measured in kPa, τ_{LOAD} the external load in Nmm and θ (the angle of rotation achieved) is measured in degrees.

The magnitude of b as a function of θ, obtained from Fig. 5, is shown in Fig. 6. These data were fitted to a second linear equation to obtain a more explicit description of pressure as a function of torque.

The resulting function for the offset, b, is

$$b(\theta) = 49.2\theta - 82.8 \tag{5}$$

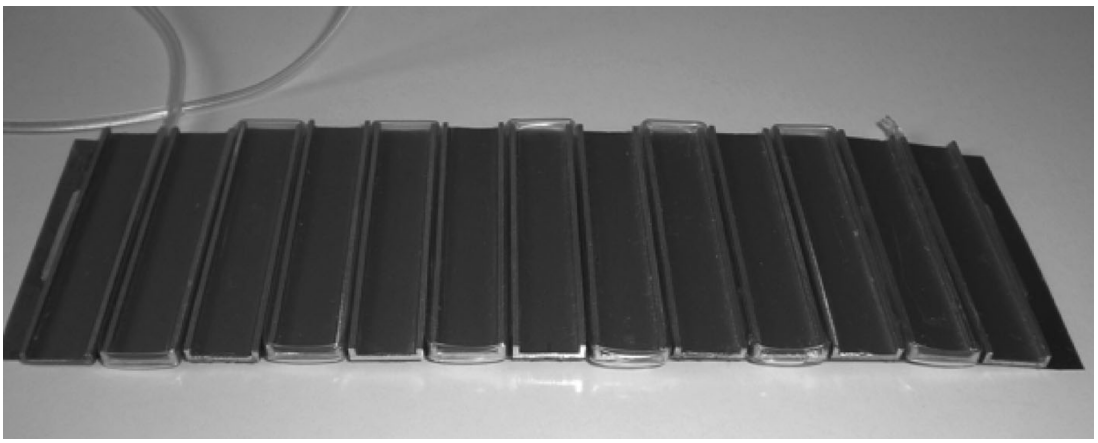

Fig. 3. Macro-scale prototype of a multi-modular hydraulic joint.

https://doi.org/10.1017/S0263574709990907 Published online by Cambridge University Press

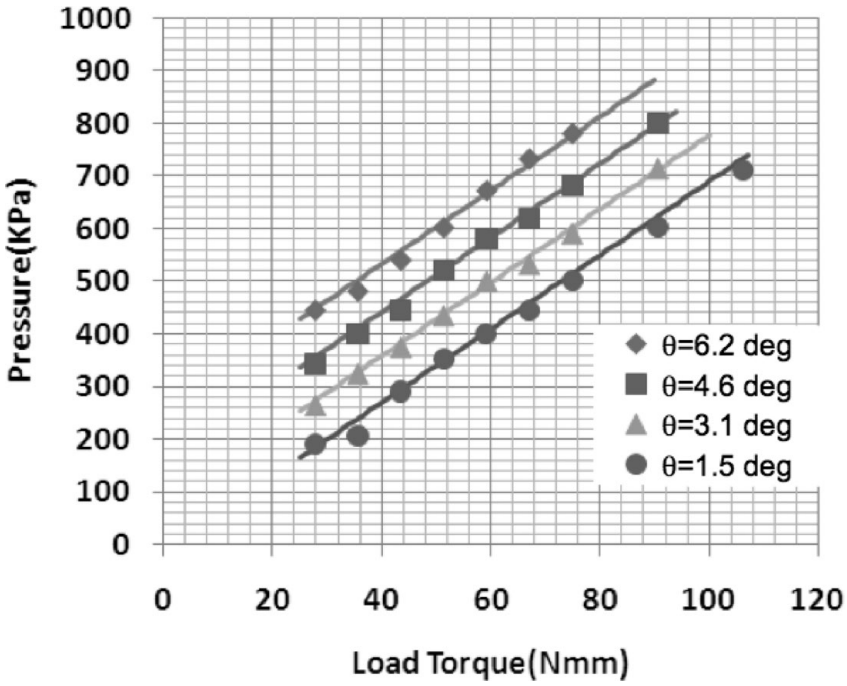

Fig. 5. Pressure plotted as a function of torque for different angles of displacement. The solid lines correspond to fitting curves defined by Eq. (4).

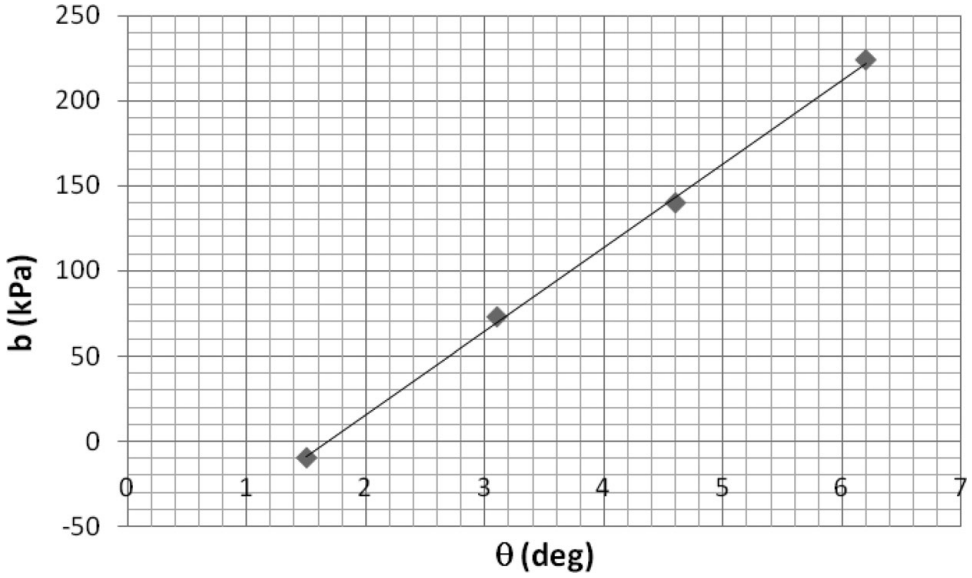

Fig. 6. The values of b plotted for different angles of rotation from trend lines of Fig. 5.

which nets a final pressure, torque, position relation,

$$p(\tau_{\mathrm{LOAD}}, \theta) = 7\tau_{\mathrm{LOAD}} + 49.2\theta - 82.8. \qquad (6)$$

The average residue between the fitting surface (Eq. (6)) and the experimental results is about 2%. It is worth mentioning that the experimental results are affected by creep and hysteresis phenomena of the hydraulic joint which are neglected in the linear modelling. The comparison between Eqs. (3) and (6) infers that the linear model, obtained under the hypothesis of small deformations, can be considered suitable to represent the static behaviour of the actuator.

4.2. Testing of an hydraulic flexible joint with multiple modules

A second series of tests were carried out in order to gauge joint efficiency and the repeated accuracy of the actuator. Seven modules were used during the experiment and four loads were tested at low pressures. The joints we clamped at one end such that they would act as a cantilevered beam. Weights ranging from 20–60 g were then affixed to the tip of the actuator and a syringe was used to inject water into the actuator tubes. The displacement of the device was then measured by analysing digital photographs, taken with a high-resolution camera, with imaging software (NI Vision Builder software).

https://doi.org/10.1017/S0263574709990907 Published online by Cambridge University Press

Fig. 7. An image of the six-module joint actuating with a 40 g load. The white and black tape was used to identify and measure that joint tip position.

Figure 7 shows the joint lifting a 40 g load with six modules. Displacement measurements were obtained from images taken by a camera perpendicular to the axis of rotation. Figure 8 illustrates the total actuator angular displacement (for six joints) given a range of pressure and three separate loads.

All three loads result in an angular displacement which is almost linear with an increase in pressure. Negative angles came about as a result of joint bending at, or near, equilibrium. Finally, data point spacing indicates that a larger load will net a smaller amount of deviation. This was investigated through repeated actuation to the same points given four different masses. Figures 9(a–d) illustrate variation about a goal displacement and equilibrium for various load values. Each test involved raising the applied pressure to a constant, consistent value, imaging the resulting displacement, and allowing it to fall back to zero. The result is a distribution of angular displacements about an average value with a variance that decreases with load.

From 20 g to 60 g, the full actuation and equilibrium displacement standard deviations are 4.1 and 2.2, 1.2 and 2.1, 1.3 and 1.5, and 0.2 and 0.4 respectively. This result confirms that higher loads net higher actuating precision.

With each angular measurement taken, syringe displacement was measured and recorded. A function was then created describing pressure and displacement length during each test. This, along with the area of the plunger, was then used to create an estimate of the applied work. Calculating the resulting work was simply a matter of obtaining the gained potential energy from raising the loads to different heights. The measured energy efficiency of the joint is displayed in the table 3.

These results only partially match the expected outcome. As a higher load would result in a lower equilibrium value angle, it was predicted that displacing the 60 g load beneath the 0 degree point would be more efficient than raising a lighter load above the axis (due to the positive effects of the compressed tubing). This turned out to only be partially true as the highest energy efficiency occurred as the 30 g load was being displaced.

4.3. Work energy model

In an effort to account for the lost energy, a model was created that documents work injected into the device and work done by the device vs. work lost to elastic deformation. Given that the compressing syringe is the only source of energy, the following equation holds true:

$$W_{\text{in}} = \int_0^x F\,\mathrm{d}s = \int_0^x A_s P_s(l)\mathrm{d}l. \tag{7}$$

Equation (7) is used in a following section when calculating overall efficiency of the actuator. A quadratic function is fit to pressure and syringe displacement data and the resulting integral is used to obtain input work. This injected energy can be used in three ways. The first is being for the deflection of each module. With only one joint, this can be expressed as,

$$W_{\text{def}} = (m_{\text{load}} + m_{\text{mod}})gs\sin(\theta) \tag{8}$$

where m_{load} is the added mass and m_{mod} is one module's mass. For multiple modules, we assume that the same angle of actuation occurs at each joint. Here we would have,

$$W_{\text{def}} = m_{\text{load}}gL\sin(\theta) + m_{\text{mod}}gs\sin(\theta)\left(\sum_{i=1}^{n} i\right) \tag{9}$$

where n is the number of modules in use. The summation in Eq. (9) accounts for the number of sections being lifted by each joint. The overall efficiency of the joint is then given by

$$\eta = \frac{W_{\text{def}}}{W_{\text{in}}}. \tag{10}$$

With actuation, energy may be dispersed through the bending of the thin elastic backing. This can be described by the relation

$$W_{\text{bend}} = \int_0^{\vartheta} \theta K_b\,\mathrm{d}\theta. \tag{11}$$

K_b, in this case, is the torsion spring constant of the thin beam. K_b was measured, rather than calculated, by bending the flexible aluminium plate with a known force

Table III. Actuator (six module) energy efficiency given a set of three different loads.

Load (g)	Max angle (deg)	Work in (J)	Work out (J)	Efficiency (%)	Max efficiency (%)
30	25.5	0.023	0.0053	25.4	25.4
40	27.18	0.175	0.0141	8.1	5.09
60	−10.87	0.075	0.0084	11.2	16.48

https://doi.org/10.1017/S0263574709990907 Published online by Cambridge University Press

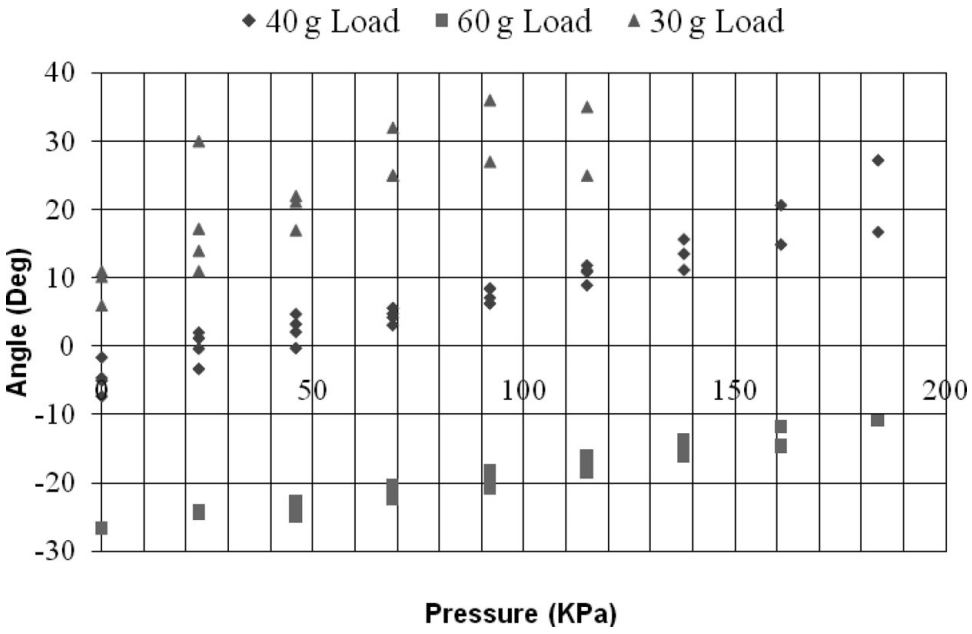

Fig. 8. Experimental results for a six-module actuator given three loads.

and recording its deflection. Finally, applied work may be lost with the deformation of the joint tubing. The tubing can be approximated as circular – when pressure is applied, it expands in a uniform manner. As a result, the two adjacent modules would displace by half the total displacement of the joint. The energy needed to cause this expansion can be estimated by considering the work needed to stretch the tubing to a new circumference. Its elastic potential energy is given by

$$W_E = \int_0^L \frac{EA\Delta L}{L_o} \mathrm{d}L \tag{12}$$

where L_o and L refer respectively to the initial and final circumference of the tubing. As such, the above can be re-written with the tube's initial and current circumference in place of length,

$$W_E = \int_0^R \frac{EA(R - R_o)}{R_o} 2\pi \mathrm{d}R. \tag{13}$$

Finally, R can be described as a function of angular displacement,

$$R = h \tan\left(\frac{\theta}{2a}\right) + R_o. \tag{14}$$

Equation (14) describes the radius of a circle given the angle $(\theta/2a)$ of a line segment (a module wall), anchored at a height h above its centre. In Eq. (14), a refers to the number of joints actively contributing to displacement. During experimentation, it was noted that not all channels contributed equally to the bending of the device. To reflect this fact, a constant a was added; it corresponds to the number of channels contributing to the final angular displacement. Integrating the elastic potential function with respect to joint displacement, θ, a final function is extracted which describes elastic work given angular displacement.

$$W_E = \frac{EAh^2\pi \tan\left(\frac{\theta}{2a}\right)}{R_o}. \tag{15}$$

Combining Eq. (15) with functions (10) and (11) nets a sum of terms describing energy as a function of angular displacement. The results of each separate work function, used to plot energy use given a 40 g load and 50% active channels, are shown in Fig. 10. The blue curve describes the work done lifting the load (obtained from the measured displacement) while the red and the green curves describe the theoretical work done to distort the tubing and bend the backing plate respectively. As the angle of displacement moves past 15°, it appears that most of the delivered energy is used to distort the tubing.

A smaller number of active channels would have netted a higher amount of energy lost to elasticity. The actuator was modelled with three active points as it was observed that most of the bending occurring happened at the centre three joints of the beam. In Fig. 11, the output work is compared to the amount of energy injected into the system. The back stars represent the measured work imparted to the system while the blue curve corresponds to the sum of the three functions plotted in Fig. 10. As work-out should be equivilant to work in, the discrepency between the two curves provides an accurate measure of the validity of the tube expansion and back plate bending energy equations.

There is an average discrepancy of 0.017 J between the two results for 10–25°. Setting the number of active channels to 2 will reduce this error to 0.005 J. However, actuation images indicate that it is unlikely that the joint is this ineffective. As such, it is likely that the unaccounted for energy was dispersed expanding the external tubing, 48 mm of which bent between actuation points. This section of the tubing was not included in the work energy model as there was no

https://doi.org/10.1017/S0263574709990907 Published online by Cambridge University Press

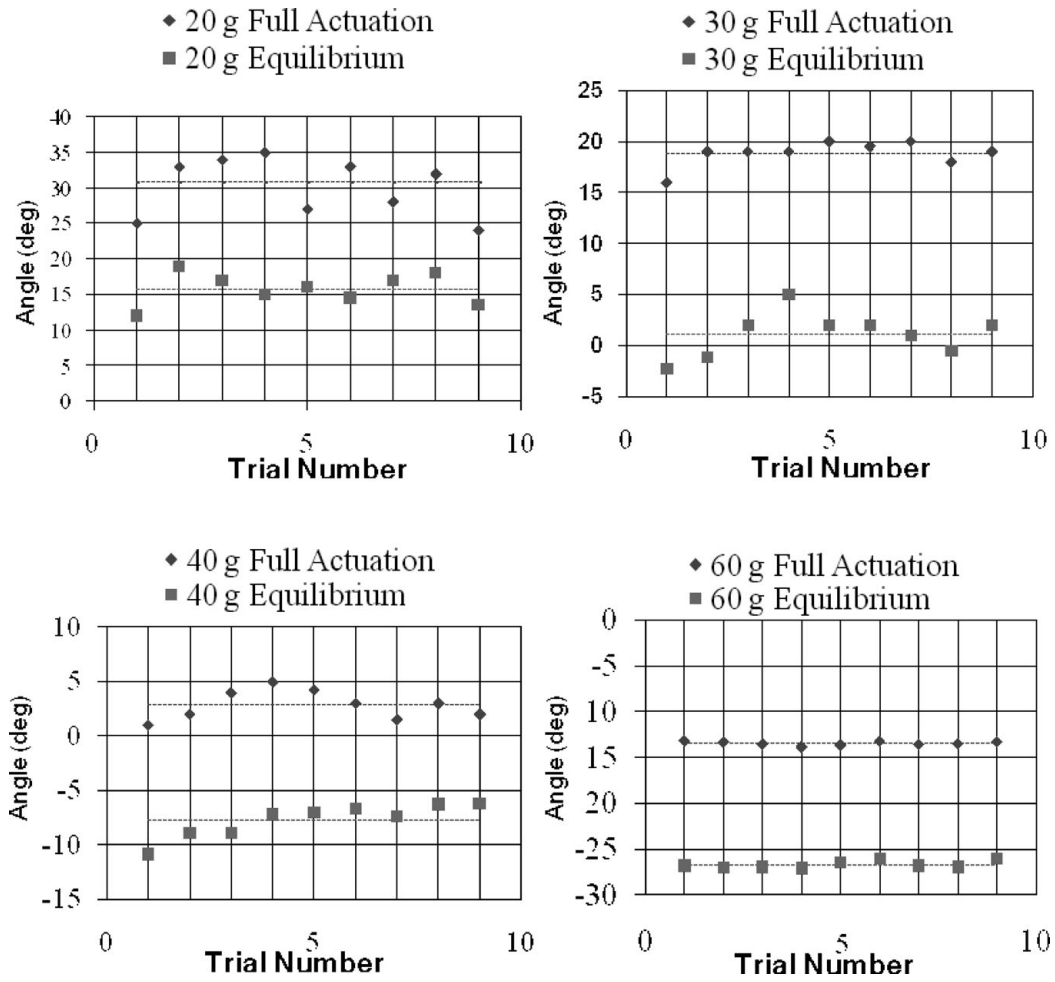

Fig. 9. (a, b, c, d) Repeatability results for 20 g, 30 g, 40 g, and 60 g respectively.

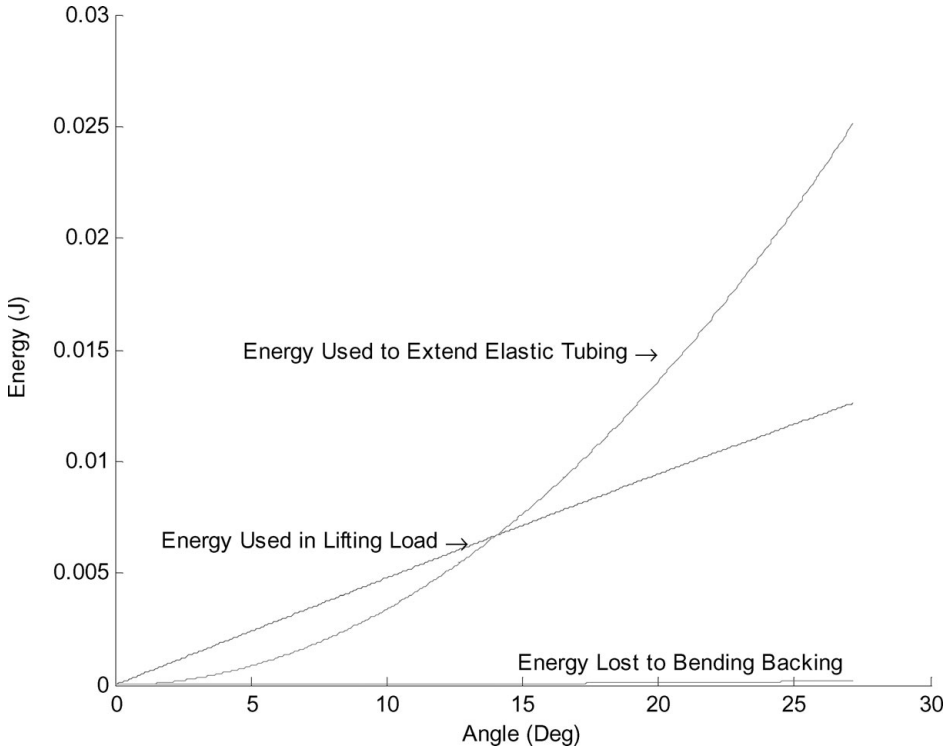

Fig. 10. Energy loss and use during actuation.

https://doi.org/10.1017/S0263574709990907 Published online by Cambridge University Press

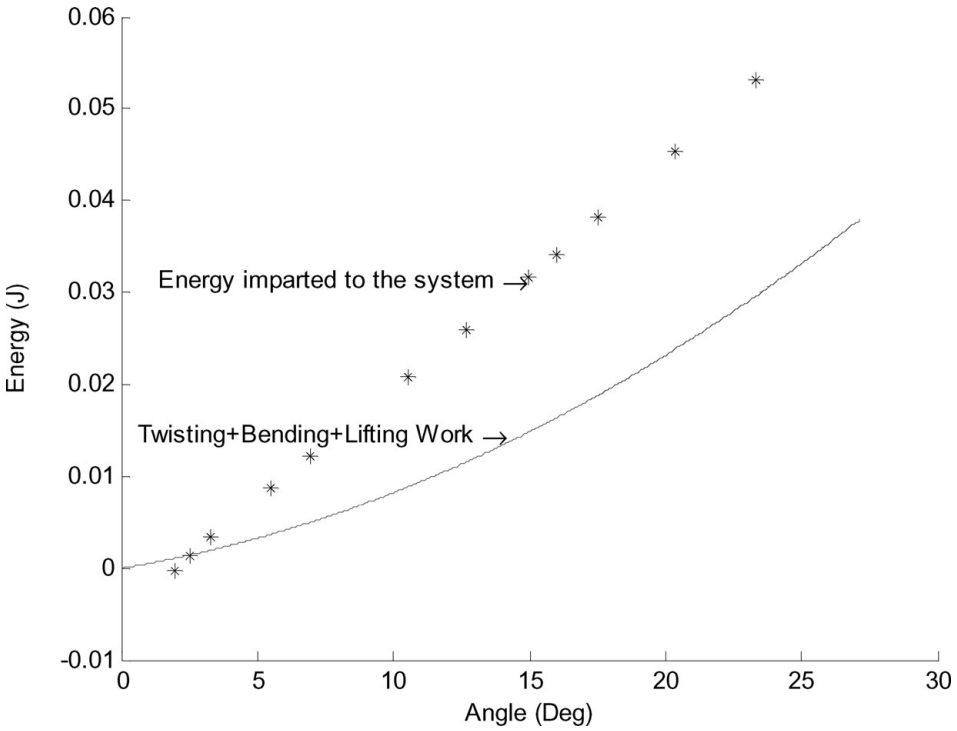

Fig. 11. Work-in compare with work-out.

simple, reliable way to predict its expansion as a function of actuator angle.

A more accurate measure of energy loss can be calculated by considering the overall efficiency of the joint. As mentioned in Section 4.2, the maximum efficiency of the joint was 5%. This indicates that 0.0095–0.0475 J of energy is lost to bending and tube expansion during actuation.

4.4. Actuator comparison

In Table IV, our device is compared with a set of common miniature rotary actuators and active joints. Three commercially available actuators (two hydrualic and one pnuematic) along with two rotary joints under development are presented. They are compared with our device using results from the one-module and seven-module tests (see the first two columns of Table IV). The key values for accurate comparison in this case are torque per unit mass, torque per unit pressure and efficiency.

The AO32 subminiature actuator is a rotationally pneumatic device that has a range of 180°.[41] It was selected as a viable comparison as it is the only commercial pneumatic device found which is of a similar physical scale (though larger in mass). It operates by exploiting the extension of two cylinders about a central rotational axis. Next is the flexator, an experimental mechanism which produces torque through the expansion of a fire hose wrapped around a rotatable cylinder.[42,43] This device demonstrates the largest torque per unit pressure of the set. The FESTO DSR/DSRL is a miniature, industrial rotary actuator. While it had a size and mass that are incomparable to the Smart Stick, it offers another example of the required torque per mass and torque factors for a commonly used robotic joint.[42,44] FMA (flexible micro actuators) refers to a class of compliant polymer

Table IV. Comparison of actuators. The acronym SFU is used to designate the actuators proposed in this paper.

Actuator	Hydraulic Actuator-1 Module	Hydraulic Actuator-7 Modules	A032 Subminiature Actuator	Flexator (42 mm × 90mm)	DSR/DSRL	FMA	Kinetrol 02–100	Units
Supplier	SFU	SFU	Rotomation	AirMuscle Ltd	Festo	Various	Kinetrol	
Mass	**0.0022**	**0.01**	0.23	0.35	1.285	0.008	0.44	kg
Max torque tested	**0.169**	**0.0105**	1.69	6.47	10	0.05	10.16	Nm
Working pressure	**543**	**180**	896.32	600	600	400	600	kPa
Torque factor	**0.000311**	**0.000058**	0.001 885	0.0108	0.0167	0.0001	0.0169	Nm/kPa
Torque per mass	**76.81**	**1.05**	7.473	18.486	7.782	6.250	23.091	Nm/kg
Max efficiency	**–**	**0.25**	–	0.5 (.67 @ 9 nm)	–	–	–	–
Length	**8**	**60**	50.8	120	126	50	70	mm
Height	**2**	**2**	39.116	63.5	92	5	76	mm
Width	**28**	**28**	38.1	–	130	5	93	mm

https://doi.org/10.1017/S0263574709990907 Published online by Cambridge University Press

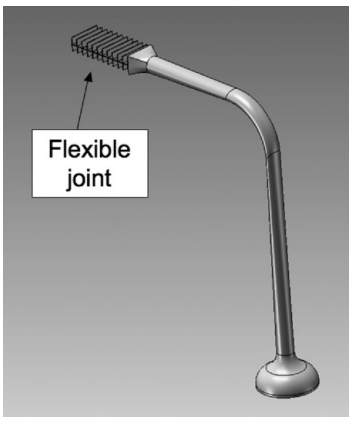

Fig. 12. Concept design of robotic leg.

actuators that are used in medical and robotic applications.[45] The quoted example is a cylindrical bellows actuator that may be used in endoluminal surgery. It is the closest in size and mass to the presented fluidic actuator. Finally, Kinetrol 02-100 is a second miniaturized hydraulic rotary actuator that has been used in industrial and robotic applications.[43]

The hydraulic actuator presented in this paper appears to fare best in the torque per unit mass and torque factor categories. And while the full device (column 2 in the table) seems to be of lower quality than the FMA device, it should be noted that it was not tested to its full abilities (upwards of 800 kPa) due to limitations of our pressure sensing equipment.

5. Feasibility of Miniaturized Legged Robot with Hydraulic Joints

Our long-term goal is to embed flexible hydraulic joints in a legged robot, which relies on bioinspired adhesive systems to climb.[35–38] In this section, the feasibility of embedding a hydraulic joint on a robotic leg is investigated. Figure 12 shows the concept design of a robotic leg with one hydraulic joint. In the following sections a static model suitable for designing the joint is presented.

5.1. Single module

A flexible hydraulic joint having a single module is considered in this section (see Fig. 13(a)). The contact area between the tube and the spacer can be computed as $A = h_1 w$ where w is the width of the flexible beam and h_1 is the height of the tube in contact with the spacer (see Fig. 13(a)). We assumed $h_1 = h$ as this configuration represents a viable implementation of the hydraulic flexible joint. In the following analysis, we consider that the pressure $p^*$is due to both the forces R and T shown in Fig. 2(b); therefore, the pressure can be expressed as $p^* = (R + T)/A$. Two instances are considered in order to investigate the feasibility of embedding the joint on a climbing robot.

The *first instance* concerns the case in which the robot lifts a leg. The stiffness of the leg is considered to be orders of magnitude higher than the stiffness of the flexible joints; the stiffness of the leg is therefore assumed to be infinite while analysing the flexible joint. The flexible joint is shown on the left side of Fig. 13(b). The torque τ_A is

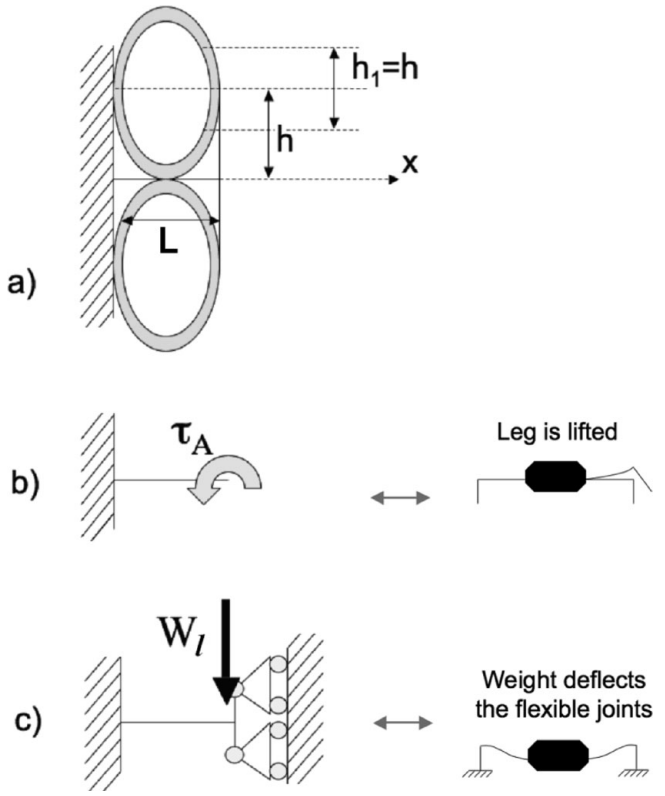

Fig. 13. (a) One module of the hydraulic joint. (b) First instance: simplified sketch with torque applied to lift a leg. (c) Second instance: simplified sketch with vertical load due to robot's weight.

assumed to be caused only by the pressurized tubes (see Fig. 13(a)) as the weight of the leg can be neglected. The case considered in this first instance can be considered as a statically determinate problem, which can be solved using classical beam theory.[32,33]

The bending angle of each single module can be computed as

$$\theta(x) = \int_0^x \frac{M}{EI} \mathrm{d}x \tag{16}$$

where θ is the bending angle of the beam due to the moment at its end (Fig. 13(b)), x is the distance from the left end of the beam connected to the ground (Fig. 13(a)), M is the moment acting on the beam, E is the Young's modulus of the beam, and I is the second moment of area of the beam, which, for a rectangular cross section, can be computed as

$$I = \frac{wt^3}{12} \tag{17}$$

where t is thickness of the beam and w is the width of the hydraulic joint.

When neglecting the transverse shear deformation[34] (i.e., using an Euler-Bernoulli beam), Eq. (16) can be used when small deformations are used. The angle θ can be computed as follows:

$$^1\theta(x) = \frac{\tau_A\, x}{E\, I} \tag{18}$$

https://doi.org/10.1017/S0263574709990907 Published online by Cambridge University Press

where the superscript i in ${}^{i}\theta(x)$ indicates the number of modules ($i = 1$ in this case). By computing the torque τ_{A} as

$$\tau_A = p^* A\, h \tag{19}$$

Eqs.(18, 19) yield

$${}^{1}\theta_{x=L} = \frac{12L\, p^*\, h^2}{E\, t^3} \tag{20}$$

The *second instance* concerns the case in which all the legs of the robot are in contact with the surface and support the weight of the robot. The weight of the robot supported by one leg, W_l, can deflect the hydraulic flexible joint. The right-hand side of Fig. 13(c) schematically shows the robot in this second instance.

Two points should be considered in order to analyse this case: (1) the large feet of the climbing robot are attached to the ground by an adhesion system – each leg can therefore be considered fixed to the ground from a static perspective; (2) the stiffness of the legs is orders of magnitude higher than the stiffness of the flexible joints – the stiffness of the leg can therefore be assumed to be infinite when the joint is analysed. As the leg can be considered infinitely stiff and fixed to the ground, one module of the flexible joint can be analysed by using the loads and constraints shown on the left-hand side of Fig. 13(c) (this figure shows the flexible joint embedded in the left leg of the robot represented on the right-hand side of Fig. 13(c)). The case represented by this second instance is a statically indeterminate problem. The deflection of the beam can be computed by solving the following differential equation

$$\frac{\mathrm{d}^2 y}{\mathrm{d}x^2} = \frac{M}{E\, I} \tag{21}$$

with the following boundary conditions:

$$\begin{cases} y = 0 & \text{for } x = 0 \\ \theta = 0 & \text{for } x = L \end{cases}. \tag{22}$$

The torque M can be represented as follows

$$M = M_C - W_l(L - x) \tag{23}$$

where M_C is a constant torque provided by the lateral constraint on the right-hand side of Fig. 13 and W_l is the weight of the robot acting upon one leg. By solving Eq. (21) and using the superposition principle, the deflection of the beam can be computed as follows:

$$y(x) = \frac{W_l x^2}{2EI}\left(\frac{x}{3} - \frac{L}{2}\right). \tag{24}$$

The maximum deflection is at $x = L$:

$$y_{x=L} = -\frac{W_l\, L^3}{12EI} \tag{25}$$

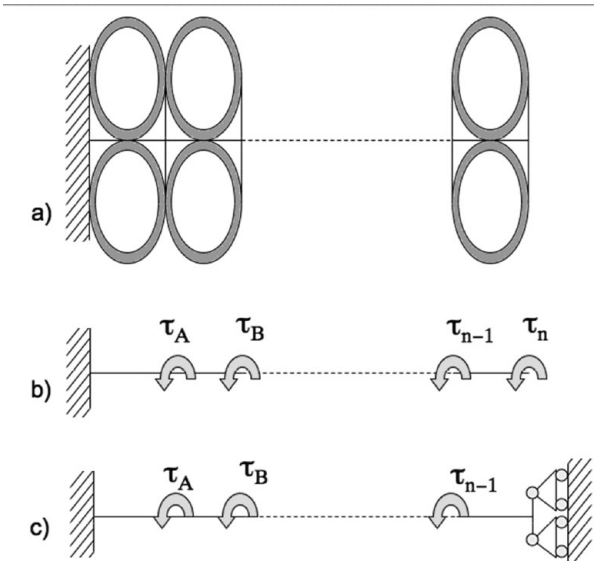

Fig. 14. Representation of a flexible joint with n modules.

Equations (20, 25), which respectively represent the first and second instance, can be used to investigate the feasibility of embedding the hydraulic flexible joint into a legged robot.

5.2. *N-module joint*

The deflection and rotation of a multi-module joint can be calculated using the above relations and knowledge of the applied torques. The flexible joint with n subsequent modules is considered in this section as a Heaviside step function:

$$H[\xi] = \begin{cases} 0 & \xi < 0 \\ 1 & \xi \geq 0 \end{cases}. \tag{26}$$

Figure 14 schematically represents this case.

The procedure presented in the previous section could be used to calculate joint motion for 2, 3, 4 to n modules. By applying an extension of the single module equations to two modules, and then extrapolating to n-modules via induction (see the Appendix), we can obtain Eqs. (27) and (28) for a flexible hydraulic joint with multiple sections:

$$\theta(x) = \frac{1}{EI}\sum_{i=1}^{n}[\tau_i x + H(x - iL) \quad \tau_i(iL - x)] \tag{27}$$

$$y(x) = \frac{1}{EI}\left\{\frac{1}{6}W_l x^3 - \frac{nW_l L x^2}{4} + \sum_{i=1}^{n-1}\left[\frac{(n-i)\tau_i x^2}{2n} + H(x - iL)\left(i\tau_i L x - \frac{\tau_i x^2}{2} - \frac{i^2}{2}\tau_i L^2\right)\right]\right\} \tag{28}$$

where n refers to the number of modules in use. Eqs. (27) and (28) are particularly relevant as they describe the static behaviour of the hydraulic flexible joint for any possible active or passive configuration for a given number of modules. They can be used to predict displacements of modular configurations, or actively control the shape of hydraulic joints embedded on the legged robotic system.

https://doi.org/10.1017/S0263574709990907 Published online by Cambridge University Press

6. Conclusion

A flexible hydraulic joint was proposed and investigated in this paper. The joint has modular design – by increasing the number of modules both displacements and rotations can be increased. A prototype was manufactured and tested. Experimental results showed close agreement between predicted hydraulic pressure, found using a simple linear model and angle and torque data, and measured internal pressure. Linear modelling was therefore considered suitable for representing the static behaviour of the joint. Quasi-static tests were carried out involving also an actuator of seven modules. Repeatability and efficiency measurements were taken. It was found that joint accuracy increases with load and its efficiency varies from 5 to 25 percent. An analytical equation for joints having *n*-modules was also derived. This equation could be used to optimally design the joint in future robotic applications.

Acknowledgments

This work was supported by the Natural Sciences and Engineering Research Council of Canada (NSERC).

References

1. J. F. Anderson and K. N. Prestwich, "The fluid pressure pumps of spiders (Chelicerata, Araneae)," *Z. Morphol Tiere* **81**, 257–277 (1975).
2. C. Menon and C. Lira, "Active articulation for future space applications inspired by the hydraulic system of spiders," *Bioinspir. Biomim.* **1**, 52–61 (2006).
3. K. Pilkauskas, R. Gaidys and C. Lira, C., "Adaptive Structures Based on Smart Stick Concept for Robotic Applications," *Proceedings of the IMAC XXV Conference on Structural Dynamics*, Orlando, Florida.
4. C. Lira and K. Pilkauskas, "Embedded Novel Actuators for Toy Applications," *Proceedings of the 6th International Conference of the European Society for Precision Engineering and Nanotechnology*, Baden bei Wien, Austria, pp. 228–231 (2006).
5. C. Lira and F. Scarpa, "Adaptive Structures for Manipulation in Clean Room," *Proceedings of SPIE 15th International Symposium on Smart Structures and Materials*, San Diego, California. Industrial and Commercial Applications of Smart Structures Technologies pp. 9–13 (2008).
6. S. Schulz, C. Pylatiuk and G. Bretthauer, "A New Ultralight Anthropomorphic Hand," *IEEE International Conference on Robotics & Automation*, Seul, Corea (2001).
7. A. Kargov, T. Asfour, C. Pylatiuk, R. Oberle, H. Klosek, S/ Schulz and K. Regenstein., "Development of an Anthropomorphic Hand for a Mobile Assistive Robot," *IEEE 9th International Conference on Rehabilitation Robotics June 28–July 1, 2005*, Chicago, IL, USA (2005).
8. S. Schulz, C. Pylatiuk, M. Reischl, J. Martin, R. Mikut and G. Bretthauer, "A hydraulically driven multifunctional prosthetic hand," *Robotica* **23**, 293–299 (2005).
9. D. Osswald, J. Martin, C. Burghart, R. Mikut, H. Wörn and G. Bretthauer, "Integrating a flexible anthropomorphic, robot hand into the control, system of a humanoid robot," *Robot. Auton. Syst.* **48**(4), 213–221 (31 Oct. 2004).
10. C. Pylatiuk, S. Schulz, A. Kargov and G. Bretthauer, "Two multiarticulated hydraulic hand prostheses," *Artif. Organs* **28**(11), 980–986 (2004).
11. A. Kargov, C. Pylatiuk, R. Oberle, H. Klosek, T. Werner, W. Roessler and S. Schulz, "Development of a Multifunctional Cosmetic Prosthetic Hand," *Proceedings of the 2007 IEEE 10th International Conference on Rehabilitation Robotics*, Noordwijk, The Netherlands (12–15 Jun. 2007).
12. K. Ikuta, H. Ichikawa, K. Suzuki and K. Yamamoto, "Micro Hydrodynamic Actuated Multiple Segments Catheter for Safety Minimally Invasive Therapy," *Proceedings of the 1003 IEEE International Conference on Robotics & Automation*, Taipei, Taiwan (14–19 Sep. 2003).
13. T. Fukuda, G. Shuxiang, K. Kosuge, F. Arai, M. Negoro and K. Nakabayashi, "Micro Active Catheter System with Multi Degrees of Freedom," *IEEE International Conference on Robotics and Automation* (1994).
14. G. Shuxiang, T. Fukuda, K. Kosuge, F. Arai, K. Oguro and M. Negoro, "Micro Catheter System with Active Guide Wire," *IEEE International Conference on Robotics and Automation* (1995).
15. K. Ikuta, H. Ichikawa, K. Suzuki and D. Yajima, "Multi-Degree of Freedom Hydraulic Pressure Driven Safety Active Catheter," *IEEE International Conference on Robotics and Automation* (2006).
16. K. Ikuta, H. Ichikawa, D. Yajima, "Hydraulic Pressure Drive with Multi-degrees of Freedom Motion for Safety Active Catheter," *IEEE International Symposium on Micro-NanoMechatronics and Human Science* (2005).
17. Y. Bailly, A. Chauvin and Y. Amirat, "Control of a High Dexterity Micro-Robot Based Catheter for Aortic Aneurysm Treatment," *IEEE Conference on Robotics, Automation and Mechatronics* (2004).
18. J. Peirs, D. Reynaerts and H. Van Brussel, "A Miniature Hydraulic Parallel Manipulator for Integration in a Self-Propelling Endoscope," *EUROSENSORS XIII The 13th European Conference on Solid-State Transducers*, The Hague, The Netherlands (12–15 Sep. 1999).
19. J. Peirs, D. Reynaerts and H. Van Brussel, "A miniature manipulator for integration in a self-propelling endoscope," *Sensors Actuators* **A 92**(1–3), 343–349 (2001).
20. R. K. Barai and K. Nonami, "Robust Adaptive Fuzzy Control Law for Locomotion Control of a Hexapod Robot Actuated by Hydraulic Actuators with Dead Zone," *Proceedings of the 2006 IEEE/RSJ International Conference on Intelligent Robots and Systems*, Beijing, China (9–15 Oct. 2006).
21. R. K. Barai and K. Nonami, "Locomotion control of a hydraulically actuated hexapod robot by robust adaptive fuzzy control and dead-zone compensation," *Robotica* **25**, 269–281 (2006) (Cambridge University Press).
22. R. K. Barai and K. Nonami, "Optimal two-degree-of-freedom fuzzy control for locomotion control of a hydraulically actuated hexapod robot," *Inf. Sci.* **177**(8), 1892–1915 (2007).
23. H. Hartikainen and K. Lehtinen, "Control and Software Structures of a Hydraulic Six-Legged Machine Designed for Locomotion in Natural Environment," *Proceedings of IEEEDSJ International Workshop on Intelligent Robots and Systems* (1992) pp. 590–596.
24. O. Becker, I. Pietsch and J. Hesselbach, "Robust task-space control of hydraulic robots," *IEEE International Conference on Robotics and Automation* (2003).
25. V. Urban, M. Wapler, J. Neugebauer, A. Hille, J. Stallkamp and T. Weisener, "Robot-assisted surgery system with kinesthetic feedback," *J. Image-Guid. Surg.* **3**(4), 205–209 (1999).
26. H. Oelhydraulik, "*HEXAMOVE Product Information* (Lucerne, Switzerland 1997).
27. S. Mutzenich, T. Vinay and G. Rosengarten, "Analysis of a novel micro-hydraulic actuation for MEMS," *Sensors Actuators* **A 116**(2004) 525–529 (2006).
28. M. De Voldera, J. Peirsa, D. Reynaertsa, J. Coosemansb, R. Puersb, O. Smalc and B. Raucentc, "A novel hydraulic microactuator sealed by surface tension," *Sensors Actuators* **A 123–124**, 547–554 (2005).
29. C. L.Wu, J. Ch.Yang, Y. Ch. Chen, "Low Power Consumption PZT Actuated Micro-Pump, Microsystems, Packaging," *Assembly Conference Taiwan, 2006. IMPACT 2006. International, IEEE* (2006) pp. 1–4.

30. D. J. Laser and J. G. Santiago, "A review of micropumps," *J. Micromech. Microeng.* **14**, R35–R64 (2004).
31. E. F. Fichter, B. L. Fichter, "A Survey of Legs of Insects and Spiders from a Kinematic Perspective," IEEE (1998).
32. F. P. Beer and E. Johnston, *Mechanics of Materials* (McGraw-Hill Book Company, 1981).
33. L. L. Howell, *Compliant Mechanisms* (Wiley, New York, 2001).
34. S. P. Timoshenko and J. M. Gere, *Theory of Elastic Stability* (McGraw Hill, 1961).
35. C. Menon, Y. Li, D. Sameoto and C. Martens, "Abigaille-I: Towards the Development of a Spider-Inspired Climbing Robot for Space Use," *IEEE RAS/EMBS International Conference on Biomedical Robotics and Biomechatronics*, Scottsdale, Arizona, USA (2008).
36. D. Sameoto, Y. Li and C. Menon, "Multi-scale compliant foot designs and fabrication for use with a spider-inspired climbing robot," *J. Bionic Eng.* **5**(3), 189–196 (2008).
37. I. Pretto, S. Ruffieux, C. Menon, A. J. Ijspeert and S. Cocuzza, "A point-wise model of adhesion suitable for real-time applications of bio-inspired climbing robots," *J. Bionic Eng.* **5**(1), 98–105 (2008).
38. C. Menon and M. Sitti, "A biomimetic climbing robot based on the gecko," *J. Bionic Eng.*, Elsevier, **3**(3), 115–125 (2006).
39. S. Kim, M. Spenko, S. Trujillo, B. Heyneman, D. Santos, M. R. Cutkosky, "Smooth vertical surface climbing with directional adhesion," *IEEE Trans. Robot.* **24**(1) (2008).
40. C. Lira, C. Menon, K. Kianfar, F. Scarpa and M. Mani, "Mining Smartness from the Hydraulic System of Spiders: A Bioinspired Actuator for Advanced Applications," *Advances in Science and Technology* (Trans Tech Publications, 2008) vol **58**, pp. 114–119.
41. Rotomation, A032 Subminiature Dual Rack Actuator, Data Sheet and Ordering Information, [Online]. Available <http://www.rotomation.com/download/minact.pdf> (Jul. 2009).
42. S. D. Prior, A. S. White, R. Gill, J. T. Parsons and P. R. Warner. A Novel Pneumatic Actuator (Advanced Manufacturing and Mechatronics Centre, Faculty of Technology, Middlesex University).
43. S. D. Prior and A. S. White, "Measurements and simulation of a pneumatic muscle actuator for a rehabilitation robot," *Simul. Pract. Theory* **3**, 81–117 (1995).
44. FSETO, DSR-DSRL Datasheet. [Online]. Available <http://www.festo.com/rep/de/assets/pdf/722824d6.pdf> (Jul. 2009).
45. A. De Greef, P. Lambert and A. Delchambre, "Towards flexible medical instruments: Review of flexible fluidic actuators," *Precis. Eng.* **33**(4), 311–321 (2009).

Appendix

In order to calculate deflections for n-modules, we begin with a two joint model. Using Eq. (15), and setting torque equal to the sum of the two joint forces, a function can be derived which describes deflection at any point x. The computation of the deflection in any point of the joint for the first load instance can be performed by using Eq. (29):

$$ {}^{2}\theta(x) = \frac{1}{EI}(\tau_1 x + \tau_2 x - H(x-L)(\tau_1 x - \tau_1 L)). \quad (29) $$

Similarly, for the second load instance, the deflection can be computed as:

$$ {}^{2}y(x) = \left(\frac{W_l x^3}{6EI} - \frac{W_l L x^2}{2EI} + \frac{\tau_1 x^2}{4EI}\right) + H(x-L)\left(\frac{\tau_1 L x}{EI} - \frac{\tau_1 L^2}{2EI} - \frac{\tau_1 x^2}{2EI}\right). \quad (30) $$

Equations (29, 30) correspond to Eqs. (18, 24), which were derived for the case of one module. By following the procedure presented in Section 5.1, but taking care in distinguishing the torque and bending locations, the rotation and deflection for a three-module actuator can be calculated. The rotation for the first load instance is

$$ {}^{3}\theta(x) = \frac{1}{EI}(\tau_1 x + \tau_2 x + \tau_3 x + H(x-L)(-\tau_1 x + \tau_1 L) + H(x-2L)(-\tau_2 x + L(\tau_1 + 2\tau_2))) \quad (31) $$

and the deflection for the second load instance is

$$ {}^{3}y(x) = \left(\frac{W_l x^3}{6EI} - \frac{3W_l L x^2}{4EI} + \frac{\tau_1 x^2}{3EI} + \frac{\tau_2 x^2}{6EI}\right) + H(x-L) \times \left(\frac{\tau_1 L x}{EI} - \frac{\tau_1 L^2}{2EI} - \frac{\tau_1 x^2}{2EI}\right) + H(x-2L) \times \left(\frac{2\tau_2 L x}{EI} - \frac{\tau_2 x^2}{2EI} - \frac{2\tau_2 L^2}{EI}\right). \quad (32) $$

Similarly, equations for the case of a joint with four modules can be derived. The rotation for the first load instance is

$$ {}^{4}\theta(x) = \frac{1}{EI}(\tau_1 x + \tau_2 x + \tau_3 x + \tau_4 x + H(x-L)(-\tau_1 x + \tau_1 L) + H(x-2L)(-\tau_2 x + L(\tau_1 + 2\tau_2)) + H(x-3L)(-\tau_3 x + L(3\tau_3 + 2\tau_2 + \tau_1))) \quad (33) $$

and the deflection for the second load instance is

$$ {}^{4}y(x) = \left(\frac{W_l x^3}{6EI} - \frac{W_l L x^2}{2EI} + \frac{3\tau_1 x^2}{8EI} + \frac{\tau_2 x^2}{4EI} + \frac{\tau_3 x^3}{8EI}\right) + H(x-L)\left(\frac{3\tau_1 x^2}{8EI} - \frac{\tau_1 L^2}{2EI} - \frac{\tau_1 x^2}{2EI}\right) + H(x-2L) \times \left(\frac{2\tau_2 L x}{EI} - \frac{\tau_2 x^2}{2EI} - \frac{2\tau_2 L^2}{EI}\right) + H(x-3L) \times \left(\frac{3\tau_3 L x}{EI} - \frac{\tau_3 x^2}{2EI} - \frac{9\tau_3 L^2}{2EI}\right). \quad (34) $$

By using mathematical induction, Eq. (27) can be obtained from Eqs. (18, 29, 31 and 33), and Eq. (28) from Eqs. (24, 30, 32 and 34).

https://doi.org/10.1017/S0263574709990907 Published online by Cambridge University Press